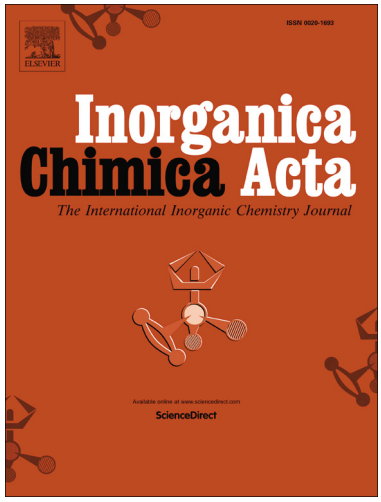

Synthesis, Structures and Aggregation-Induced Emissive Properties of Copper(I) Complexes with 1H-imidazo[4,5-f][1,10]phenanthroline Derivative and Diphosphine as Ligands

Rong Liu, Miao-Miao Huang, Xi-Xi Yao, Hao-Huai Li, Feng-Lei Yang, Xiu-Ling Li

PII: S0020-1693(15)00281-9
DOI: http://dx.doi.org/10.1016/j.ica.2015.05.019
Reference: ICA 16549

To appear in: *Inorganica Chimica Acta*

Received Date: 19 April 2015
Revised Date: 22 May 2015
Accepted Date: 22 May 2015

Please cite this article as: R. Liu, M-M. Huang, X-X. Yao, H-H. Li, F-L. Yang, X-L. Li, Synthesis, Structures and Aggregation-Induced Emissive Properties of Copper(I) Complexes with 1H-imidazo[4,5-f][1,10]phenanthroline Derivative and Diphosphine as Ligands, *Inorganica Chimica Acta* (2015), doi: http://dx.doi.org/10.1016/j.ica.2015.05.019

Synthesis, Structures and Aggregation-Induced Emissive Properties of Copper(I) Complexes with 1H-imidazo[4,5-f][1,10]phenanthroline Derivative and Diphosphine as Ligands

Rong Liu, Miao-Miao Huang, Xi-Xi Yao, Hao-Huai Li, Feng-Lei Yang, Xiu-Ling Li*

School of Chemistry and Chemical Engineering & Jiangsu Key Laboratory of Green Synthetic Chemistry for Functional Materials, Jiangsu Normal University, Xuzhou, Jiangsu 221116, China
**Corresponding author: E-mail: lxl@jsnu.edu.cn*

Abstract

Reaction of 4-bromo-2-(1H-imidazo[4,5-f][1,10]phenanthrolin-2-yl)phenol (BIPP), chelating diphosphine ligands and $[Cu(MeCN)_4]ClO_4$ afforded five mononuclear $[Cu(BIPP)(PP)]ClO_4$ (PP = dppe, **1**; dppp, **2**; bdpp, **3**; POP, **4**; xantphos, **5**) complexes with good phosphorescent emission in the solid state. All the complexes are characterized by elemental analyses, electrospray Ionization mass spectra, ^1H and ^{31}P NMR spectra and X-ray single crystallography. The photoluminescence quantum yields of complexes **1–5** are from 0.0067 to 0.2616 in the solid state under air atmosphere, which increase with the increasing rigidity of diphosphine ligands and the increasing strength of intermolecular and intramolecular π···π interactions. The aggregation-induced emission of complexes **4** and **5** at room temperature was investigated.

Keywords: Copper(I) complexes, 1H-imidazo[4,5-f][1,10]phenanthroline derivative, crystal structure, aggregation-induced emission

1. Introduction

Luminescent materials with aggregation-induced emission (AIE) have attracted much attention since 2001 and have been developed into a novel class of fluorescent turn-on biosensors with superior sensitivity [1−3]. Most AIE systems focused on organic luminescent molecules [1−5], on the other hand, the heavy-metal

complexes that possess d^6 [6–18], d^8 [19–22], and d^{10} electron configurations showed strong spin–orbit coupling, resulting in efficient phosphorescence emission. The relative long emission lifetimes of phosphorescence provide these heavy-metal complexes a chance as bioimaging probes to eliminate autofluorescence from biological sample through time-gated technique. Aggregation-induced phosphorescence emission (AIPE) provides a good path to active the luminescent behaviour of the metal complexes with twisting ligands in the solution. However, most reported AIPE systems were focused on Ir(III) [7–18], Pt(II) [19–22], and Au(I) systems [23–29]. The limited availability, toxicity and the prices of these systems will limit their wide application in bioimaging probes. Therefore, it is necessary and urgent to explore, design and synthesize noble-metal-free AIPE complexes. In this purpose, copper(I) complexes containing diimine and diphosphine ligands appear to be a good alternative [30].

Cu(I)-diimine-phosphine systems in luminescent family have received more and more attention in the past 36 years since the early work of McMilin's group was reported [30–37]. It was found that some Cu(I)-diimine-diphosphine complexes showed intense phosphorescent emission behavior in the solid state, but they were non-emissive or weakly emissive in the fluid environment due to the emission cancellation resulting from oxygen and intramolecular motions including rotation and vibration, especially within the twisted diphosphine ligands, which served as a relaxation channel for the excited states to deactivate [30, 34d, 35c]. Therefore, AIE phenomenon provides a new way for the application of Cu(I)-diimine-diphosphine systems as ''turn-on'' luminescent materials by taking the advantage of luminogenic aggregation through restriction of intramolecular motion in the aggregated state. We reported a series of mononuclear and binuclear Cu(I)-diimine-diphosphine complexes with good phosphorescent properties at room temperature [30, 34d, 35c], and the binuclear $[Cu_2(BrphenBr)_2(Ph_2P(CH_2)_nPPh_2)_2](ClO_4)_2$ (BrphenBr = 3,8-dibromo-1,10-phenanthroline) complexes exhibited good AIPE behavior and were further used for living

cell imaging successfully [30]. As a phenanthroline (phen) derivative, 4-bromo-2-(1H-imidazo[4,5-f][1,10]phenanthrolin-2-yl)phenol (BIPP) not only possesses the chelating phenanthroline (phen) coordination sites, but also possesses the possible intramolecular hydrogen bond between hydroxyl group and nitrogen atom of the imidazole ring. Such intramolecular hydrogen bond increases the rigidity of BIPP, which restricts the intramolecular rotations, and thus might improve the luminescence behavior of its Cu(I) complexes. As our continuous effort to exploit the Cu(I)-diimine-diphosphine luminescent systems, herein we report the syntheses, structures and AIE properties of a series of copper(I) complexes with BIPP and diphosphine as ligands.

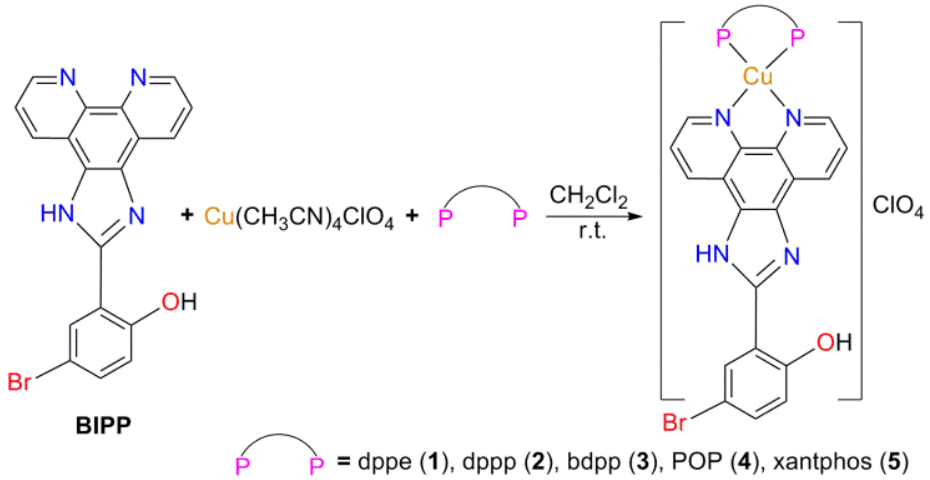

Scheme 1. Synthetic routes to complexes **1**–**5**.

2. Experimental Section

2.1. Materials and reagents

The reagents 5,6-diamino-1,10-phenanthroline (dap), 1,2-bis(diphenylphosphino)ethane (dppe), 1,3-bis(diphenylphosphino)propane (dppp), 1,2-bis(diphenylphosphino)benzene (bdpp), bis[(2-diphenylphosphino)phenyl] ether (POP) and 9,9-dimethyl-4,5-bis(diphenylphosphino)-9H-xanthene

(xantphos) were commercially available and were used without further purification. $[Cu(CH_3CN)_4]ClO_4$ was prepared by the published method [38]. All solvents were purified and distilled by suitable procedures before use. All other reagents were of analytical grade and were used as received. All samples used for studying the spectra and properties are powders from crystals which were milled and then dried under infrared light.

2.2. Instruments

^1H and ^{31}P NMR spectra were obtained from the solutions in DMSO-d_6 using a Bruker-400 spectrometer with Me_4Si as an internal standard and 85% H_3PO_4 as an external standard, respectively (see Figures S1–S11). UV-Vis absorption spectra were determined on a Purkinje General TU-1901 UV-vis spectrophotometer. Electrospray Ionization Mass Spectra (ESI-MS) analyses were carried out with a Bruker-micro-TOFQ-MS analyzer using a DCM/methanol mixture for the mobile phase. Elemental analyses (C, H, and N) were carried out on a Perkin–Elmer model 240C elemental analyzer. Steady-state excitation and emission spectra were obtained with a Hitachi F4500 fluorescence spectrophotometer. Emission lifetimes were measured on an Edinburgh FLS920 fluorescence spectrometer under air atmosphere. The photoluminescence yields in the solid state under air atmosphere at room temperature is defined as the ratio of number of photons emitted to the number of photons absorbed by the system and was measured under air with pure solid and an empty sphere on an Edinburgh analytical instrument FLS920 with an integrating sphere established by Wrighton et al [39]. The excitation wavelengths used for emission lifetimes and photoluminescence yields were 355, 350, 350, 330 and 330 nm, respectively, for complexes **1**–**5**. The emission wavelengths used for emission lifetimes were 601, 570, 531, 552 and 544 nm, for complexes **1**–**5**. The data of emission lifetimes were fitted basing on the single exponential fitting mode. The exponential function used for fitting the data was $y = y_0 + A^{-x/t}$. The Chi-squares are 0.98549, 0.99813, 0.99705, 0.99786 and 0.99799, respectively, for complexes **1**–**5**. The

emission wavelength range used for determining photoluminescence yields were 340−800 nm, 335−800 nm, 335−800 nm, 315−800 nm and 315−800 nm, for complexes **1**–**5**, respectively.

2.3. Single Crystal X-Ray Determination

Suitable single crystals were picked from the hexane/DCM systems in diffusive equilibrium, and then they were quickly wrapped in epoxy resin or petroleum jelly and transferred to a stream of cold N_2 on Bruker Smart APEX II diffractometer fitted with a CCD-type area detector. The data were collected using graphite-monochromatised Mo-Kα radiation (λ = 0.71073 Å). The CrystalClear software package 2009, Bruker SAINT was used for data reduction [40, 41]. The absorption corrections were applied using SADABS supplied by Bruker [42]. In all cases the structures were solved by direct methods and refined by the full-matrix least-squares method on F^2 data using the SHELXTL–97 program package [43]. Heavy atoms were found from the E-map, and the remaining non-hydrogen atoms were located in subsequent Fourier maps. Non-hydrogen atoms of complexes **1**–**5** were refined with anisotropic thermal parameters, while hydrogen atoms were generated geometrically and refined with isotropic thermal parameters riding on those of the parent atoms.

2.4. Preparation of BIPP and complexes

All reactions for complexes were carried out under anaerobic conditions using standard Schlenk techniques under an atmosphere of dry argon at room temperature.

2.4.1. BIPP

BIPP was prepared by a modified procedure [44, 45]. The mixture of 5-bromosalicylaldehyde (1.00 mmol, 1 equiv), dap (1.00 mmol, 1 equiv), five drops of hydrogen peroxide H_2O_2 (30% aqueous) and three drops of

HOAc (2.00 mol·L^{-1}) was refluxed in ethanol (20 mL) for 12 h. After completion of the reaction, the mixture was cooled to room temperature and the solvent was concentrated in vacuo. After filtration, the yellow desired precipitate was washed by cold ethanol and dried in vacuo. Yield: 73%. ^{1}H NMR (400 MHz, DMSO-d_6, δ, ppm): 13.997 (s, 1H, NH), 12.852 (s, 1H, OH), 9.064 (br, 2H), 8.879 (d, J = 7.6 Hz, 2H), 8.370 (d, J = 2.4 Hz, 1H), 7.849 (s, 2H), 7.533 (dd, J = 8.8 Hz, J' = 2.0 Hz, 1H), 7.061 (d, J = 8.4 Hz, 1H).

*2.4.2. [Cu(bipp)(dppe)]ClO_4·CH_2Cl_2 (**1**·CH_2Cl_2)*

[Cu(CH_3CN)$_4$]ClO_4 (32.6 mg, 0.100 mmol) was added to a degassed DCM solution (about 10 mL) of BIPP (39.1 mg, 0.100 mmol) and dppe (40.6 mg, 98%, 0.100 mmol). A pale yellow suspension was obtained quickly and then stirred for 2 h at room temperature. After filtration, layering *n*-hexane dropwise onto the DCM solution carefully produced the product as pale yellow crystals a few weeks later in 52% yield (53.4 mg). Anal. Calcd for $C_{45}H_{35}BrClCuN_4O_5P_2$ (**1**) (950.025): C 56.84, H 3.71, N 5.90. Found: C 56.57, H 3.65, N 5.81. ESI-MS (*m/z*): 853.0740 [Cu(BIPP)(dppe)]$^+$ (calcd 853.0747). ^{1}H NMR (400 MHz, DMSO-d_6, δ, ppm): 14.100 (s, 1H, NH), 12.462 (s, 1H, OH), 9.151 (d, J = 6.4 Hz, 2H), 8.958 (d, J = 4.4 Hz, 2H), 8.122 (br, 3H), 7.544–7.344 (m, 19H), 7.271–7.098 (m, 2H), 6.654 (s, 1H), 2.826 (t, 4H, J = 6.2 Hz, PCH_2). ^{31}P NMR {^{1}H NMR} (400 MHz, DMSO-d_6, δ, ppm): –4.081.

*2.4.3. [Cu(bipp)(dppp)]ClO_4·2CH_3CN (**2**·2CH_3CN).*

This compound was prepared by the same synthetic procedure as that of **1** except for using dppp instead of dppe. Color: pale yellow. Yield: 81%. Anal. Calcd for $C_{46}H_{37}BrClCuN_4O_5P_2$ (**2**) (964.041): C 57.26, H 3.87, N 5.81. Found: C 57.03, H 3.92, N 5.74. ESI-MS (*m/z*): 867.094 [Cu(BIPP)(dppp)]$^+$ (calcd 867.090). ^{1}H NMR (400 MHz, DMSO-d_6, δ, ppm): 14.164 (s, 1H, NH), 12.477 (s, 1H, OH), 9.200–9.140 (m, 4H), 8.238–8.137 (m, 3H), 7.383–7.185 (m, 21H), 6.757 (br, 1H), 2.900 (br, 4H, PCH_2), 2.095 (m, 2H, PCH_2CH_2). ^{31}P NMR {^{1}H NMR} (400 MHz, DMSO-d_6, δ, ppm): –12.511.

*2.4.4. [Cu(bipp)(bdpp)]$ClO_4 \cdot CH_2Cl_2$ (**3**$\cdot CH_2Cl_2$)*

This compound was prepared by the same synthetic procedure as that of **1** except for using bdpp instead of dppe. Color: orange yellow. Yield: 35%. Anal. Calcd for $C_{49}H_{35}BrClCuN_4O_5P_2$ (**3**) (998.025): C 58.92, H 3.53, N 5.61. Found: C 59.03, H 3.61, N 5.68. ESI-MS (*m/z*): 901.067 $[Cu(BIPP)(bdpp)]^+$ (calcd 901.075). ^{1}H NMR (400 MHz, DMSO-d_6, δ, ppm): 14.042 (s, 1H, NH), 12.314 (s, 1H, OH), 9.069 (s, 2H), 8.640 (s, 1H), 8.592 (s, 1H), 8.044–7.993 (m, 3H), 7.819–7.797 (m, 2H), 7.650–7.628 (m, 2H), 7.513–7.422 (m, 12H), 7.343–7.137 (m, 8H), 6.998–6.539 (m, 2H). ^{31}P NMR {^{1}H NMR} (400 MHz, DMSO-d_6, δ, ppm): −3.725.

*2.4.5. [Cu(bipp)(POP)]$ClO_4 \cdot 2.5CH_2Cl_2$ (**4**$\cdot 2.5CH_2Cl_2$)*

This compound was prepared by the same synthetic procedure as that of **1** except for using POP instead of dppe. Color: yellow. Yield: 73%. Anal. Calcd for $C_{55}H_{39}BrClCuN_4O_6P_2$ (**4**) (1090.051): C 60.55, H 3.61, N 5.14. Found: C 60.23, H 3.70, N 5.06. ESI-MS (*m/z*): 993.095 $[Cu(BIPP)(POP)]^+$ (calcd 993.101). ^{1}H NMR (400 MHz, DMSO-d_6, δ, ppm): 14.218 (s, 1H, NH), 12.504 (s, 1H, OH), 9.119 (d, J = 7.6 Hz, 2H), 8.883 (d, J = 4.4 Hz, 2H), 8.373 (s, 1H), 7.945 (s, 2H), 7.512–6.976 (m, 28H), 6.701–6.663 (m, 2H). ^{31}P NMR {^{1}H NMR} (400 MHz, DMSO-d_6, δ, ppm): −11.667.

*2.4.6. [Cu(bipp)(xantphos)]$ClO_4 \cdot 2CH_2Cl_2$ (**5**$\cdot 2CH_2Cl_2$)*

This compound was prepared by the same synthetic procedure as that of **1** except for using xantphos instead of dppe. Color: yellow. Yield: 53%. Anal. Calcd for $C_{58}H_{43}BrClCuN_4O_6P_2$ (**5**) (1130.08): C 61.59, H 3.83, N 4.96. Found: C 61.72, H 3.81, N 4.89. ESI-MS (*m/z*): 1033.11 $[Cu(BIPP)(xantphos)]^+$ (calcd 1033.13). ^{1}H NMR (400 MHz, DMSO-d_6, δ, ppm): 14.236 (s, 1H, NH), 12.466 (s, 1H, OH), 9.108 (d, J = 8.0 Hz, 2H), 8.546 (d, J = 4.4 Hz, 2H), 8.389 (s, 1H), 7.940–7.889 (m, 4H), 7.588–7.522 (m, 1H), 7.314–7.234 (m, 6H), 7.138–7.017 (m, 9H), 6.942–6.930 (m, 8H), 6.598–6.580 (m, 2H), 1.775 (s, 6H, CH_3). ^{31}P NMR {^{1}H NMR} (400 MHz, DMSO-d_6, δ, ppm): −12.822.

3. Results and discussion

3.1. Syntheses of the ligand BIPP and the Cu(I) complexes

Biswas's group reported the synthesis of 2-substituted benzimidazoles at ambient temperature from various alkyl and aryl aldehydes using 3,6-di(pyridine-2-yl)-1,2,4,5-tetrazine (pytz) as catalyst and aerial oxygen as oxidants under visible light irradiation [44]. Chen et al synthesized BIPP by refluxing the mixture of 5,6-diamino-1,10-phenanthroline (dap) and 5-bromosalicylaldehyd in ethanol for 12h [45]. Here, BIPP was prepared by a modified procedure using dap and 5-bromosalicylalde as starting materials, hydrogen peroxide (H_2O_2) as the oxidant and HOAc as the catalyst without light irradiation. Complexes **1–5** (Scheme 1) were synthesized in good yields by reaction of an equimolar BIPP, diphosphine ligands (dppe = 1,2-bis(diphenylphosphino)ethane, dppp = 1,3-bis(diphenylphosphino)propane (dppp), bdpp = 1,2-bis(diphenylphosphino)benzene, POP = bis[(2-diphenylphosphino)phenyl] ether, xantphos = 9,9-dimethyl-4,5-bis(diphenylphosphino)-9H-xanthene) and $[Cu(CH_3CN)_4]ClO_4$ in dichloromethane (DCM) solution. All the complexes crystallized with solvent molecules. Once formed, they are stable to air and moisture in the solid state.

3.2. Crystallographic studies

The corresponding crystallographic data and selected refinement details of all the complexes are presented in Table 1. Selected bond lengths and angles are listed in Table 2. ORTEP drawings of the cations for complexes **1–5** are depicted in Figures 1–5, respectively. All the Cu(I) centers in complexes **1–5** adopt distorted tetrahedral coordinated geometries completed by N_2P_2 donor atoms with two N atoms from BIPP and two P atoms from chelating diphosphine ligands. Such distortion mainly originates from the rigid BIPP ligand, which restricts the N–Cu–N bite angles to 81.62(11)°, 80.60(17)°, 82.08(14)°, 80.93(15)° and 81.10(15)°, and 80.52(10)° for complexes **1–5**, respectively. The corresponding P–Cu–P angles are 90.61(4)°,

103.08(6)°, 90.43(5)°, 113.00(5)° and 114.97(5)°, and 121.55(3)° for complexes **1**–**5**, respectively, showing much variation to each other with different diphosphine ligands. The dihedral angles between N–Cu–N and P–Cu–P planes are 86.61(8)°, 86.93(12)°, 76.81(12)°, 85.19(11)° and 85.64(11)°, and 80.76(8) for complexes **1**–**5**, respectively. Both the larger P–Cu–P angles and the smaller dihedral angles between N–Cu–N and P–Cu–P planes imply that the PPh_2 groups in the corresponding complexes are sterically much closer to the BIPP ligands [30, 37g].

Table 1. Crystallographic data and select refinement details for **1**·CH_2Cl_2, **2**·2CH_3CN, and **3**·CH_2Cl_2, **4**·2.5CH_2Cl_2 and **5**·2CH_2Cl_2.

	1·CH_2Cl_2	**2**·2CH_3CN	**3**·CH_2Cl_2	**4**·2.5CH_2Cl_2	**5**·2CH_2Cl_2
Empirical formula	$C_{46}H_{37}BrCl_3CuN_4O_5P_2$	$C_{50}H_{43}BrClCuN_6O_3P_2$	$C_{50}H_{37}BrCl_3CuN_4O_2P_2$	$C_{57.5}H_{44}BrCl_6CuN_4O_6P_2$	$C_{60}H_{47}BrCl_3CuN_4O_6P_2P_2$
Formula weight	1037.54	1048.74	1085.58	1305.06	1302.66
T (K)	150(2)	150(2)	150(2)	150(2)	150(2)
Wavelength (Å)	0.71073	0.71073	0.71073	0.71073	0.71073
Crystal system	triclinic	monoclinic	monoclinic	monoclinic	triclinic
Space group	*P*–1	*P*2(1)/c	*P*2(1)/c	*P*2(1)/c	*P*–1
Unit cell dimensions					
a (Å)	13.0541(4)	17.7043(5)	11.2997(4)	20.2683(3)	12.2897(3)
b (Å)	13.6044(5)	13.7292(4)	17.9383(7)	15.6090(3)	14.9638(4)
c (Å)	15.3763(5)	21.2556(6)	24.5882(8)	39.8830(6)	17.2244(4)
α (°)	106.348(2)				105.9040(10)
β (°)	111.353(2)	107.899(2)	115.968(2)	117.5540(10)	109.7680(10)
γ(°)	104.241(2)				97.3010(10)
V (Å^3)	2247.26(13)	4916.4(2)	4480.8(3)	11186.5(3)	2781.01(12)
Z	2	4	4	8	2
D_{calc} (mg·m^{-3})	1.533	1.417	1.609	1.550	1.556
μ (mm^{-1})	1.676	1.429	1.685	1.504	1.466
F(000)	1052	2144	2200	5287	1324
Reflections collected	33095	35993	34092	86057	39921
Independent reflections	7875	6891	7860	19660	9734
Reflections with $I > 2\sigma$(I)	6295	4711	6176	15736	8802
Data/restraints/parameters	7875/0/559	6891/32/619	7860/0/590	19660/12/1416	9734/0/712
Goodness-of-fit (GOF) on F^2	1.045	1.013	1.027	1.063	1.030
Final R indices [$I > 2\sigma$(I)]	0.0483	0.0578	0.0578	0.0655	0.0497
wR_2 [$I > 2\sigma$(I)]	0.1353	0.1512	0.1454	0.1603	0.1408
R indices (all data)	0.0621	0.0907	0.0784	0.0834	0.0544
wR_2 (all data)	0.1462	0.1759	0.1601	0.1725	0.1456

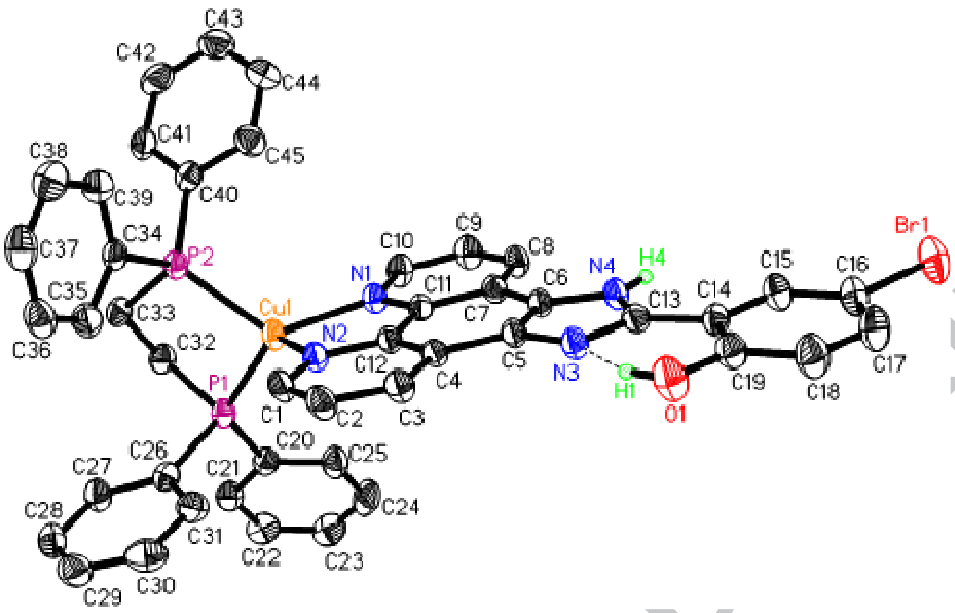

Fig. 1. ORTEP drawings of complex **1**·CH_2Cl_2 with the atom labelling scheme, showing 30% thermal ellipsoids. Most hydrogen atoms are omitted for clarity. (d(O1−H1···N3) = 2.564 Å, ∠ O1−H1···N3 = 149°)

Table 2. Selected bond lengths (Å) and angles (°) for **1**·CH_2Cl_2, **2**·$2CH_3CN$, and **3**·CH_2Cl_2, **4**·$2.5CH_2Cl_2$ and **5**·$2CH_2Cl_2$.

	1·CH_2Cl_2	**2**·$2CH_3CN$	**3**·CH_2Cl_2	**4**·$2.5CH_2Cl_2$	**5**·$2CH_2Cl_2$
Cu1–N1	2.044(3)	2.071(4)	2.021(4)	2.091(4)	2.105(3)
Cu1–N2	2.051(3)	2.048(4)	2.049(4)	2.044(4)	2.052(3)
Cu2–N5				2.058(4)	
Cu2–N6				2.079(4)	
Cu1–P1	2.243(1)	2.239(2)	2.245(1)	2.211(1)	2.314(1)
Cu1–P2	2.244(1)	2.221(2)	2.228(1)	2.304(1)	2.250(1)
Cu2–P3				2.307(1)	
Cu2–P4				2.211(1)	
N1–Cu1–N2	81.62(11)	80.60(17)	82.08(14)	80.93(15)	80.52(10)
N5–Cu2–N6				81.10(15)	
P1–Cu1–P2	90.61(4)	103.08(6)	90.43(5)	113.00(5)	121.55(3)
P3–Cu2–P4				114.97(5)	
N1–Cu1–P1	122.88(9)	115.88(13)	115.01(11)	133.77(11)	96.13(8)
N1–Cu1–P2	123.11(9)	129.34(13)	134.18(11)	97.67(11)	124.16(8)
N2–Cu1–P1	124.80(9)	105.25(13)	125.29(12)	122.06(11)	109.10(8)
N2–Cu1–P2	117.81(9)	119.94(13)	114.69(11)	102.28(11)	117.14(8)
N5–Cu2–P3				101.57(11)	
N5–Cu2–P4				120.57(11)	
N6–Cu2–P3				97.81(11)	
N6–Cu2–P4				133.16(11)	

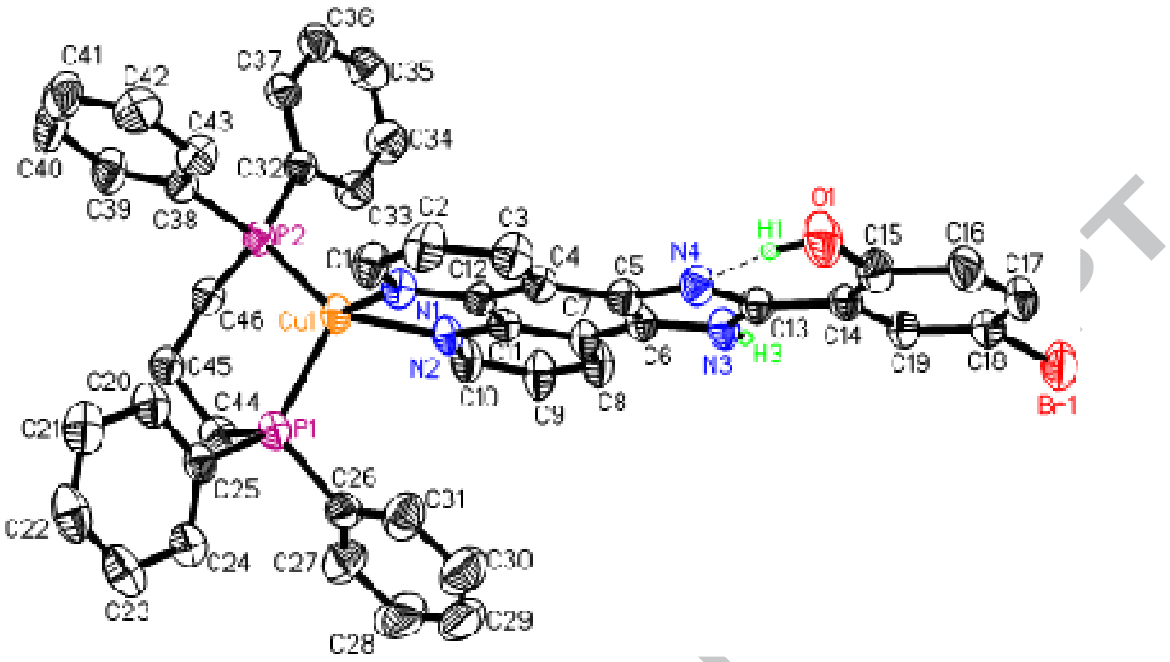

Fig. 2. ORTEP drawings of complex **2**·2CH_3CN with the atom labelling scheme, showing 30% thermal ellipsoids. Most hydrogen atoms are omitted for clarity. (d(O1–H1···N4) = 2.613 Å, ∠ O1–H1···N4 = 146°)

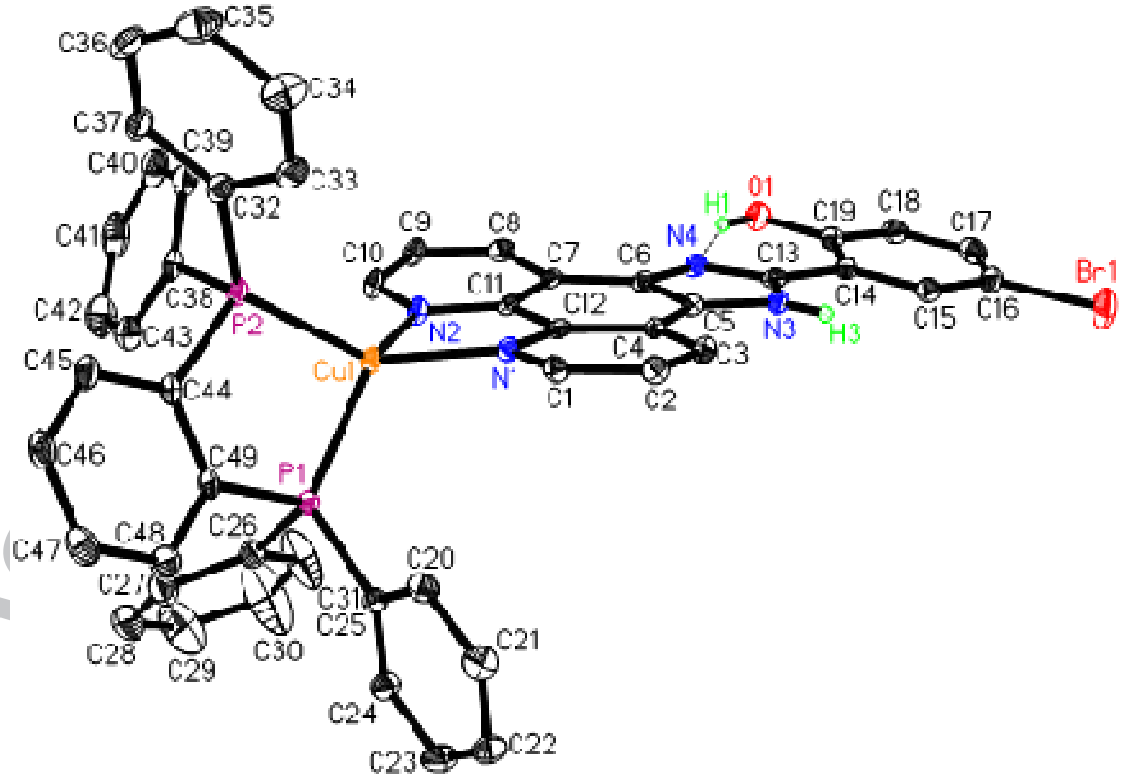

Fig. 3. ORTEP drawings of complex **3**·CH_2Cl_2 with the atom labelling scheme, showing 30% thermal ellipsoids. Most hydrogen atoms are omitted for clarity. (d(O1–H1···N4) = 2.597 Å, ∠ O1–H1···N4 = 148°)

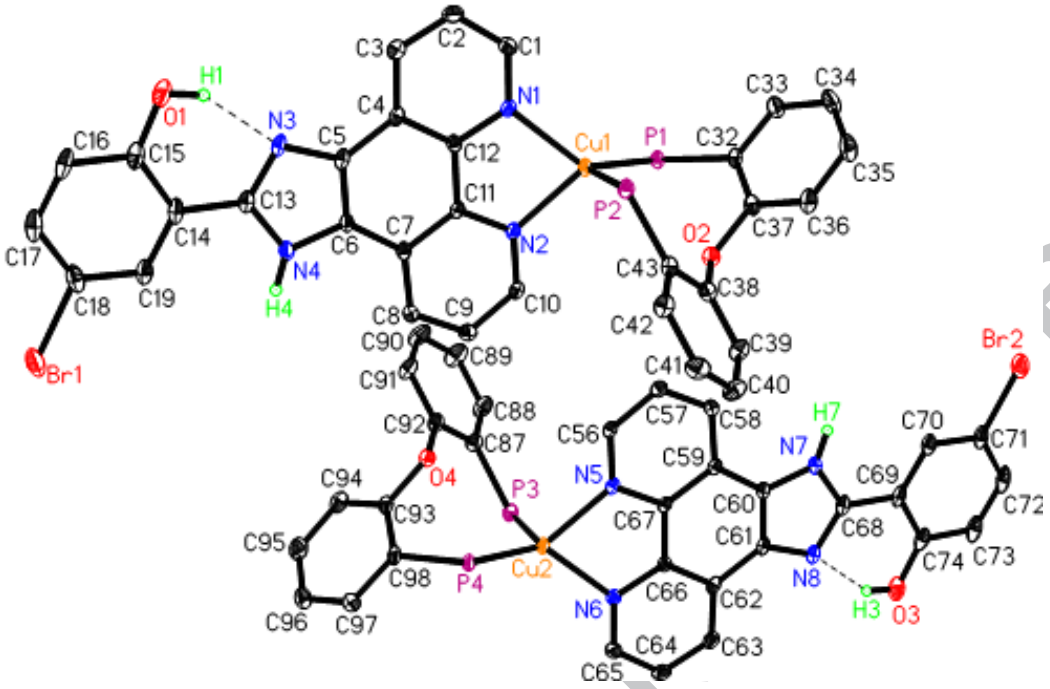

Fig. 4. ORTEP drawings of two asymmetric cations of complex **4**·2.5CH_2Cl_2 with the atom labelling scheme, showing 30% thermal ellipsoids. Most hydrogen atoms and some phenyl rings are omitted for clarity. (d(O1−H1···N3) = 2.641 Å, ∠ O1−H1···N3 = 148°; d(O3−H3···N8) = 2.648 Å, ∠ O3−H3···N8 = 148°)

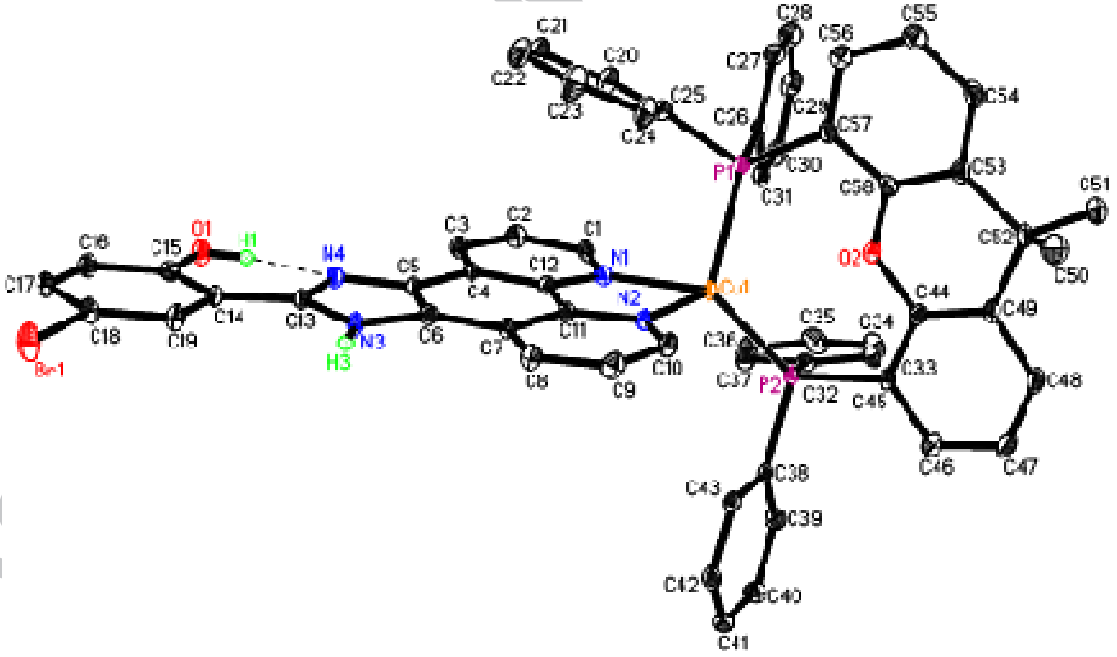

Fig. 5. ORTEP drawings of complex **5**·2CH_2Cl_2 with the atom labelling scheme, showing 30% thermal ellipsoids. Most hydrogen atoms are omitted for clarity. (d(O1−H1···N4) = 2.602 Å, ∠ O1−H1···N4 = 148°)

The Cu–N and Cu–P bond distances fall in range of 2.021(4) – 2.105(3) Å and 2.211(1) – 2.314(1) Å, respectively, which are comparable to those observed in other Cu(I)-diimine-diphosphine complexes [30, 32–37]. The average Cu–N distances are 2.048, 2.060, 2.035, 2.068 and 2.079 Å for complexes **1–5**, respectively, with the shortest average Cu–N distance occurring at complex **3** and the longest average distance occurring at complex **5**. While the average Cu–P bond lengths are 2.244, 2.230, 2.237, 2.258 and 2.282 Å for complexes **1–5**, respectively, with the shortest average Cu–P distance occurring at complex **1** and the longest average distance occurring at complex **5**. The longest Cu–N and Cu–P bond lengths for complex **5** among the series indicate that the largest repulsion between BIPP and diphosphine ligands occurs in complex **5** because of the bulky xantphos. The ligand BIPP in each copper(I) cation keeps good coplanity with dihedrals between phenyl ring and 1H-imidazo[4,5-f][1,10]phenanthroline plane being 3.6° for complex **1**, 5.3° for complex **2**, 7.0° for complex **3**, 1.7° and 2.4° for complex **4**, 3.8° for complex **5**, respectively. In addition, in all complexes, phenolic hydroxyl groups link with the N atoms through O–H···N hydrogen bonds with O ···N distances in the range of 2.564 – 2.648 Å and O–H···N angles in the range of 146° – 149° (see Figures 1–5 and Table S1). The N–H bonds in the imidazole rings link with perchlorate ions through N–H···O hydrogen bonds with N ···O distances in the range of 2.830 – 2.882 Å and N–H···O angles in the range of 156° – 171° (see Table S1). Such intramolecular hydrogen bonds improve the rigidity of BIPP.

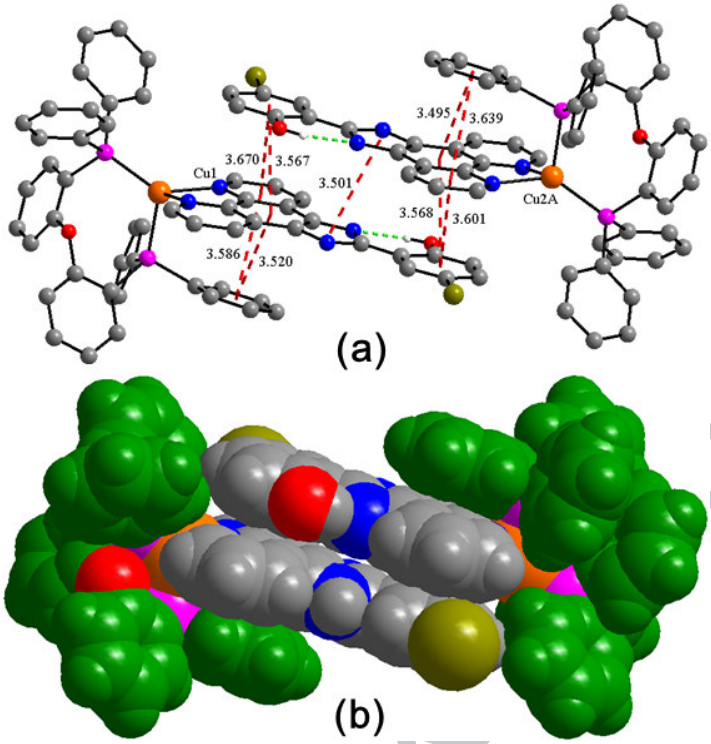

Fig. 6. The cation dimer of complex **4** formed through intermolecular and intramolecular π···π interactions. (a) Ball-and-stick model (Most hydrogen atoms are omitted for clarity. symmetry code for A: *x*, *y* + 1, *z*); (b) the space-fillings (C and H atoms of pop are shown with green color and those of BIPP are shown with grey color for clarity).

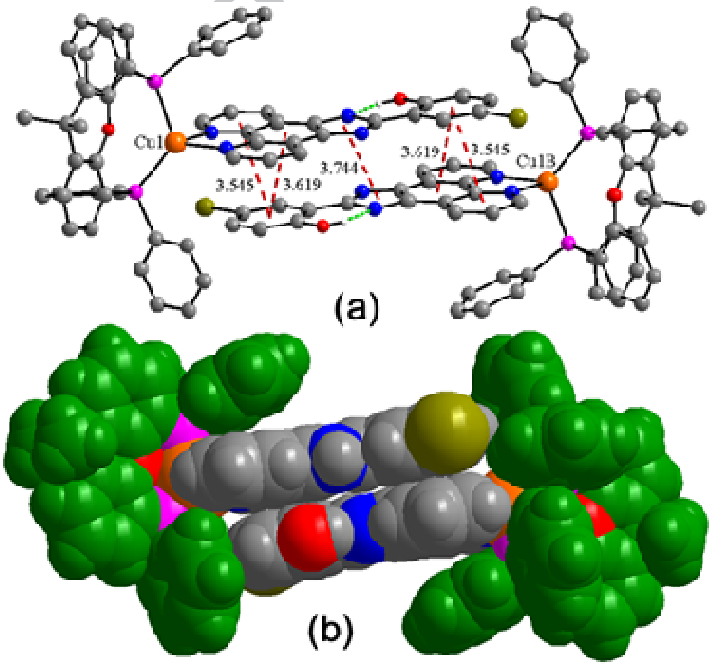

Fig. 7. The cation dimer of complex **5** formed through intermolecular π···π interactions. (a) Ball-and-stick model (Most hydrogen atoms are omitted for clarity. symmetry code for B: −*x*, −*y* + 1, −*z* + 1); (b) the space-fillings (C and H atoms of xantphos are shown with green color and those of BIPP are shown with grey color for clarity).

On the other hand, as shown in Figures 6–7, Figures S12–S14 and Table S2, intermolecular π···π interactions widely exist between BIPP molecules, leading to the formation of the cation dimers. Quadruple, triple, quintuple, quintuple and quintuple intermolecular π···π interactions were observed in complexes **1**–**5**, respectively, between phenyl rings and phen rings, and between imidazole rings, with the distances between ring centroids in the range of 3.458–3.781 Å. Furthermore, double intramolecular π···π interactions were also observed between phen rings and phenyl rings of POP in complex **4** with the distances between ring centroids in the range of 3.495–3.639 Å. The copper(I) centers can be more effectively protected by BIPP and diphosphine ligands from the attack of oxygen and solvent molecules due to such intermolecular and intramolecular π···π interactions along with the larger P–Cu–P angles and the smaller dihedral angles between N–Cu–N and P–Cu–P planes. The well protected Cu(I) centers can also be seen from the space-fillings of cation dimers of complexes **1**–**5** in Figures 6 and 7 and Figures S12–S14 (see supporting information). The best protected Cu(I) centers are suggested to be in complexes **4** and **5**. Such good protection make complexes **1**–**5** are very stable to air and moisture in the solid state.

3.3. Photophysical Properties

3.3.1. Absorption spectra

Table 3. Photophysical data of complexes **1**–**5** at room temperature.

compd	λ_{abs}/nm (ε/M^{-1}cm^{-1}) (CH_2Cl_2)	λ_{em}/nm (solid)	τ_{em}/μs (solid)	Φ_{em} (solid)
1	229 (68400), 280 (60920), 339 (27480), 354 (24440), 428 (8520)	601	4.55±0.04	<1.0%
2	229 (69240), 280 (65800), 340 (29400), 354 (27080), 421 (8320)	570	7.25±0.02	<1.0%
3	230 (78160), 281 (66040), 339 (30200), 352 (26960), 431 (9640)	531	7.67±0.03	(12.4±1.0)%
4	230 (78600), 280 (76080), 339 (33560), 352 (30960), 411 (9040)	552	14.24±0.05	(9.0±1.1)%
5	230 (79280), 280 (85080), 340 (32520), 353 (30520), 411 (8840)	544	17.70±0.06	(26.2±1.0)%

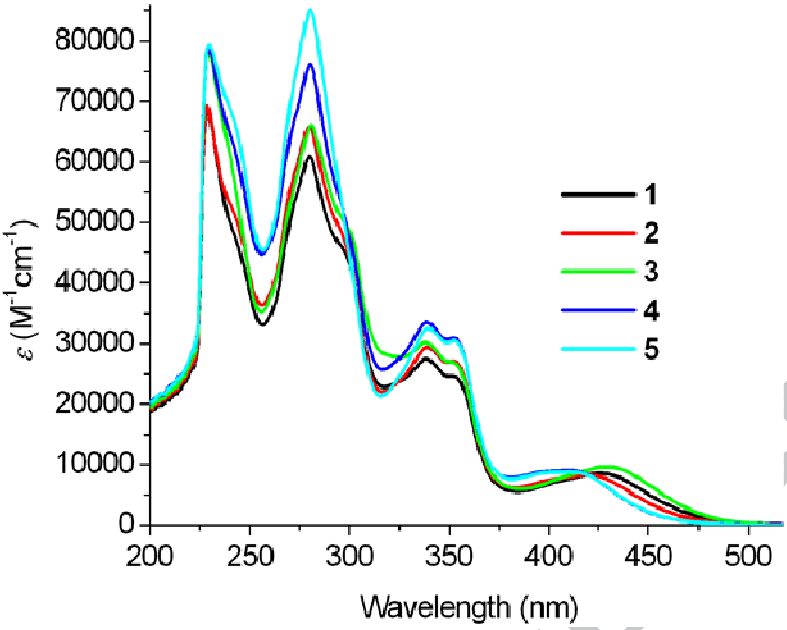

Fig. 8. UV-vis absorption spectra of **1**–**5** in DCM at room temperature.

UV-vis absorption data of complexes **1**–**5** in DCM solutions with concentrations at 2.500×10^{-5} mol·L^{-1} at room temperature are summarized in Table 3, while the corresponding electronic absorption spectra are depicted in Figure 8. The molar extinction coefficients are calculated basing on the UV-vis absorption spectra of the solutions with 1.000×10^{-5} and 2.500×10^{-5} mol·L^{-1}. The maximum absorbance of 2.500×10^{-5} mol·L^{-1} solutions are at about 2.000. Too low concentration results in the increase of the dissociation of the complexes, and too high concentration won't obey Beer-Lambert's Law. For this series, the solutions obey Beer-Lambert's Law with the concentration in the range of 1.000×10^{-5}–2.500×10^{-5} mol·L^{-1}. All the complexes display strong absorption peaks (molar extinction coefficient $\varepsilon > 10^4$ M^{-1} cm^{-1}) with wavelengths shorter than 360 nm that can be assigned to intraligand $\pi\rightarrow\pi^*$ transitions of both BIPP and diphosphine ligands. The lower-energy absorption bands with maximum wavelengths in the range of 411–431 nm and ε in the range of 8320–9640 M^{-1} cm^{-1} are assigned to $d\pi$(Cu)$\rightarrow\pi^*$(diimine) metal-to-ligand charge transfer (MLCT) transitions, mixing with some charge transfer character from diphosphine ligand to diimine ligands within the cation. Such assignments base on the results of density functional theory (DFT) calculation of

complex [Cu(dmbpm)(POP)]BF_4 (dmbpm = 4,4′-dimethyl-2,2′-bipyrimidine), which showed the frontier orbitals of [Cu(dmbpm)(POP)]BF_4, LUMO and LUMO+1 were located mainly at dmbpm, and HOMO and HOMO−1 were mainly centered on the copper and POP [46].

3.3.2. Photoluminescence (PL) in the Solid State

The excitation and emission spectra of complexes **1**–**5** in the crystalline state were investigated at room temperature (see Figure 9), and the corresponding spectral data, including emission wavelengths, emission lifetimes, and the photoluminescence quantum yields in the solid state under air atmosphere are listed in Table 3. Complexes **1**–**5** display moderate to intense emission bands with λ_{max} = 601, 570, 531, 552 and 544 nm, respectively. The emission bands span a wide wavelength range resulting in rich emission color. The microsecond range lifetimes are consistent with $d\pi$(Cu)→π^*(diimine) (^{3}MLCT) transitions as the origin of the emission bands [30, 34c, 35d]. The replacement flexible dppe, dppp and POP by more rigid diphosphine ligands bdpp and xantphos leads to the obvious enhancement of emission quantum yields from 0.0067 (complex **1**), 0.0106 (complex **2**), 0.0895 (complex **4**) to 0.1239 (complex **3**) and 0.2616 (complex **5**). The richer intermolecular and intramolecular π···π interactions in complex **4** along with a larger P–Cu–P bite angle may play a key role for the enhancement of the luminescence behavior compared with complexes **1** and **2** since π···π interactions and large P–Cu–P bite angles provide good protection for the Cu(I) centers from the attack of oxygen [30, 35c].

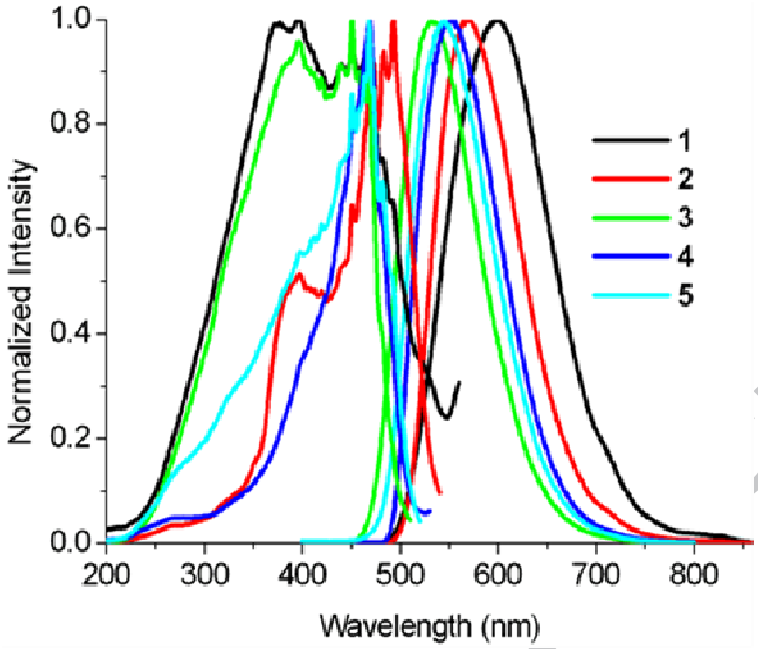

Fig. 9. The PL excited (left) and emission spectra of complexes **1**–**5** (right) in the solid state at room temperature.

3.3.3. Aggregation-Induced Emission

In pure DCM solutions, only was complex **5** observed with weak emission under the radiation at 365 nm in air atmosphere, and all other complexes shows no obvious emission. The non-emissive behavior of complexes **1**–**4** and the weak emission of complex **5** in DCM solutions are suggested to arise from the luminescence quenching caused by oxygen and the active intramolecular motions (rotation and vibration) [1, 30, 47]. Both the very weak emission in the solution and intense luminescent behavior in the solid state suggest that complexes **1**–**5** may show AIE behavior. Here, complexes **4** and **5** were selected for AIE studies. In order to investigate their AIE attributes, different amounts of hexane, a poor solvent for complexes **4** and **5**, were added to the DCM solutions by defining the hexane volume fractions (f_h) of 0–90% and keeping the concentrations constant at 5.000×10^{-5} mol·L^{-1}. Figure 10 shows the AIE spectra of complexes **4** and **5** for different f_h with the excitation wavelength at 330 nm with optical filter at 395 nm. The AIE luminescent images of **4** and **5** with different f_h and those in the solid state under 365 nm radiation are shown in Figure 11.

No obvious emission in the DCM–hexane mixture with a hexane fraction (f_h) less than 70% for complex **4** and 75% for complex **5**, respectively, was observed. Raising the hexane content to 70% and 75% for complexes **4** and **5** induces the complexes to aggregate obviously and leads to dramatic luminescence enhancement (Figures 10 and 11). As shown in Figure 10, complexes **4** and **5** exhibit good AIE behavior with the most intense emission appearing at f_h = 80% and 85%, respectively. Since complexes **4** and **5** were insoluble in hexane, increasing the hexane fraction in the mixed solvent would change their existing forms from a solution in DCM to the aggregated particles in the DCM/hexane mixed solvent, so enhanced emission intensity was observed due to aggregation. The further addition of hexane to 85% for complex **4** and 90% for complex **5**, however, resulted in a lowering of the luminescence intensity, which may be attributed to an increase of the particle size since the increase of the particle size would prevent the formation of the well-disperse aggregation state and lead to the precipitation. Complexes **4** and **5** exhibit various AIE colors changing from yellow-green to yellow. Similar AIE effect was also observed for the binuclear $[Cu_2(BrphenBr)_2(Ph_2P(CH_2)_nPPh_2)_2](ClO_4)_2$ (BrphenBr = 3,8-dibromo-1,10-phenanthroline) complexes with common features of twisted structures and freely rotatable peripheral aromatic moieties [30]. It's worth mentioning that yellow-green AIE luminescence of complex **4** contrasts markedly with the yellow emission in the solid state (see Figure 11), indicating that AIE colors depend on the different aggregation states dramatically**.** Here, the restriction of intramolecular motion (RIM), which includes rotation and vibration, is proposed to be the main cause for the AIE behavior of complexes **1**–**5**.

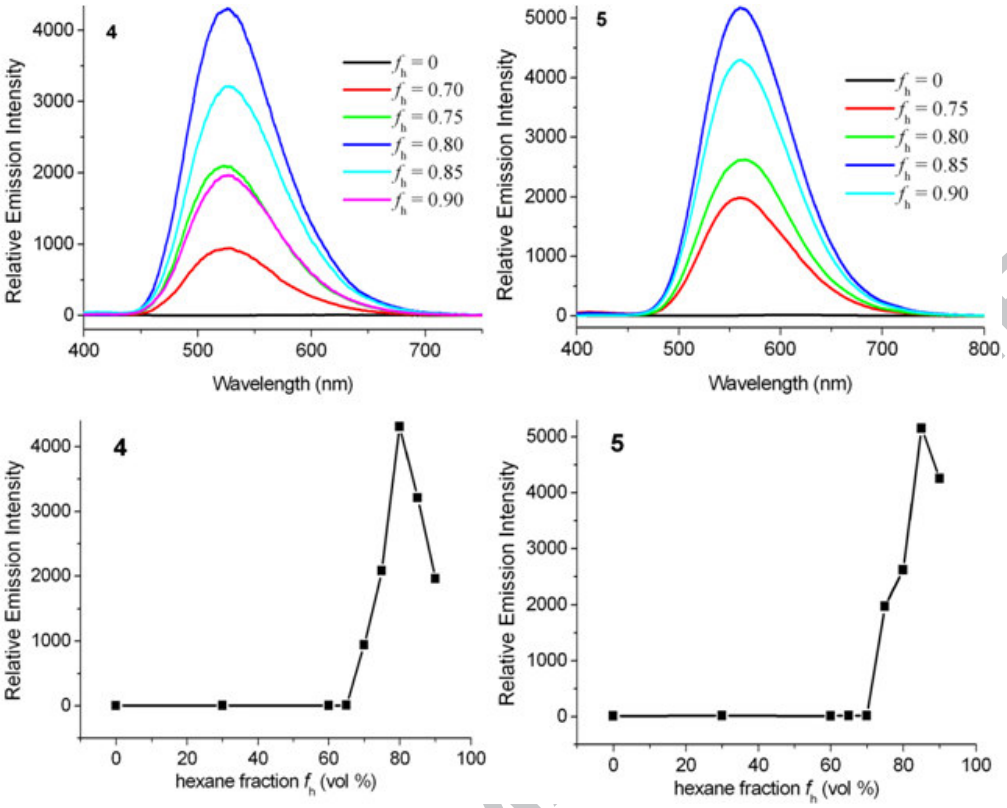

Fig. 10. AIE spectra of **4** and **5** in DCM/hexane mixed solvents (up) and the change of peak intensity (down) with different f_h with the excitation at 330 nm.

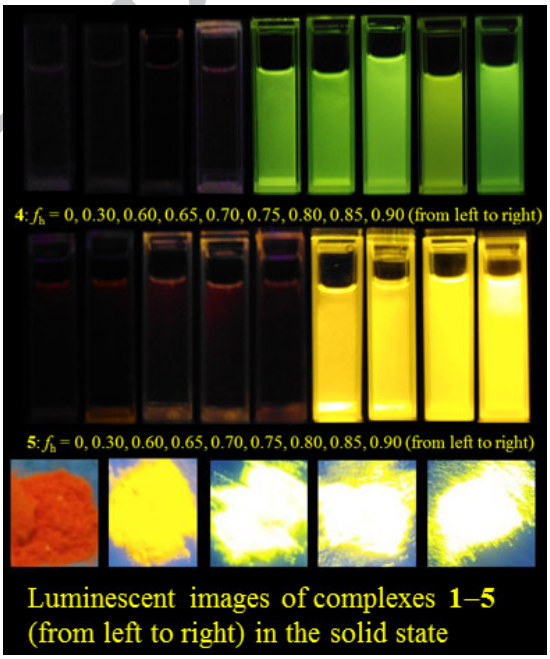

Fig. 11. AIE luminescent images of **4** and **5** in hexane-DCM mixed solvents with the concentration kept at 5.000×10^{-5} mol·L^{-1} and luminescence images of complexes **1**–**5** in the solid state radiated with an ultraviolet light at 365 nm.

4. Conclusions

Five mononuclear [Cu(BIPP)(PP)]ClO_4 complexes with good phosphorescent emission in the solid state were synthesized and characterized. The photoluminescence quantum yields of complexes **1–5** in the solid state under air atmosphere increase with the increasing rigidity of diphosphine ligands and the increasing strength of intermolecular and intramolecular π···π interactions. Complexes **4** and **5** displayed good aggregation-induced emission behaviour at room temperature.

Acknowledgements

This work is supported financially by the National Natural Science Foundation of China (21271091 and 21401086), the Major Basic Research Project of Natural Science Foundation of the Jiangsu Higher Education Institutions (11KJA430009), and PAPD of Jiangsu Higher Education Institutions.

Appendix A. Supplementary material

CCDC 1046965−1046969 contains the supplementary crystallographic data for complexes **1**·CH_2Cl_2, **2**·2CH_3CN, **3**·CH_2Cl_2, **4**·2.5CH_2Cl_2 and **5**·2CH_2Cl_2**.** These data can be obtained free of charge via http://www.ccdc.cam.ac.uk/conts/retrieving.html, or from the Cambridge Crystallographic Data Centre, 12 Union Road, Cambridge CB2 1EZ, UK; fax: (+44) 1223-336-033; or e-mail: deposit@ccdc.cam.ac.uk. Supplementary data associated with this article can be found, in the online version, at ??????.

References

[1] R. T. K. Kwok, C. W. T. Leung, J. W. Y. Lam, B. Z. Tang, Chem. Soc. Rev. 44 (2015) DOI: 10.1039/C4CS00325J

[2] R. Hu, N. L. C. Leung, B. Z. Tang, Chem. Soc. Rev. 43 (2014) 4494.

[3] Y. Hong, J. W. Y. Lam, B. Z. Tang, Chem. Soc. Rev. 40 (2011) 5361.

[4] E. Zhao, J. W. Y. Lam, L. Meng, Y. Hong, H. Deng, G. Bai, X. Huang, J. Hao, B. Z. Tang, Macromolecules 48 (2015) 64.

[5] Y. Cai, K. Samedov, B. S. Dolinar, Z. Song, B. Z. Tang, C. Zhang, R. West, Organometallics 34 (2015) 78.

[6] Y. Chen, W. C. Xu, J. F. Kou, B. L. Yu, X. H. Wei, H. Chao, L. N. Ji, Inorg. Chem. Commun. 13 (2010) 1140.

[7] Y. Wu, H. Z. Sun, H. T. Cao, H. B. Li, G. G. Shan, Y. A. Duan, Y. Geng, Z. M. Su, Y. Liao, Chem. Commun. 50 (2014) 10986.

[8] G. Li, Y. Wu, G. Shan, W. Che, D. Zhu, B. Song, L. Yan, Z. Su, M. R. Bryce, M. Su, Y. Liao, Chem. Commun. 50 (2014) 6977.

[9] X. G. Hou, Y. Wu, H. T. Cao, H. Z. Sun, H. B. Li, G. G. Shan, Z. M. Su, Chem. Commun. 50 (2014) 6031.

[10] G. G. Shan, H. B. Li, J. S. Qin, D. X. Zhu, Y. Liao, Z. M. Su, Dalton Trans. 41 (2012) 9590.

[11] G. G. Shan, L. Y. Zhang, H. B. Li, S. Wang, D. X. Zhu, P. Li, C. G. Wang, Z. M. Su, Y. Liao, Dalton Trans. 41 (2012) 523.

[12] G. G. Shan, D. X. Zhu, H. B. Li, P. Li, Z. M. Su, Y. Liao, Dalton Trans. 40 (2011) 2947.

[13] P. Alam, G. Kaur, C. Climent, S. Pasha, D. Casanova, P. Alemany, C. A. Roy, I. R. Laskar, Dalton Trans. 43 (2014) 16431.

[14] P. Alam, M. Karanam, D. Bandyopadhyay, A. R. Choudhury, I. R. Laskar, Eur. J. Inorg. Chem. 2014 (2014) 3710.

[15] P. Alam, P. Das, C. Climent, M. Karanam, D. Casanova, A. R. Choudhury, P. Alemany, N. R. Jana, I. R. Laskar, J. Mater. Chem. C 2 (2014) 5615.

[16] K. S. Bejoymohandas, T. M. George, S. Bhattacharya, S. Natarajan, M. L. P. Reddy, J. Mater. Chem. C 2 (2014) 515.

[17] C. H. Shin, J. O. Huh, S. J. Baek, S. K. Kim, M. H. Lee, Y. Do, Eur. J. Inorg. Chem. (2010) 3642.

[18] Q. Zhao, L. Li, F. Li, M. Yu, Z. Liu, T. Yi, C. Huang, Chem Commun. (2008) 685.

[19] S. S. Pasha, P. Alam, S. Dash, G. Kaur, D. Banerjee, R. Chowdhury, N. Rath, C. A. Roy, I. R. Laskar, RSC Advances 4 (2014) 50549.

[20] H. Honda, J. Kuwabara, T. Kanbara, J. Organomet. Chem. 772–773 (2014) 139.

[21] H. Honda, Y. Ogawa, J. Kuwabara, T. Kanbara, Eur. J. Inorg. Chem. 2014 (2014) 1865.

[22] S. Liu, H. Sun, Y. Ma, S. Ye, X. Liu, X. Zhou, X. Mou, L. Wang, Q. Zhao, W. Huang, J. Mater. Chem. 22 (2012) 22167.

[23] Z. Chen, J. Zhang, M. Song, J. Yin, G. A. Yu, S. H. Liu, Chem. Commun. 51 (2015) 326.

[24] Y. Guo, X. Tong, L. Ji, Z. Wang, H. Wang, J. Hu, R. Pei, Chem. Commun. 51 (2015) 596.

[25] J. Liang, Z. Chen, L. Xu, J. Wang, J. Yin, G. A. Yu, Z. N. Chen, S. H. Liu, J. Mater. Chem. C 2 (2014) 2243.

[26] J. Liang, Z. Chen, J. Yin, Yu, G. A. Yu, S. H. Liu, Chem. Commun. 49 (2013) 3567.

[27] G. G. Shan, H. B. Li, H. Z. Sun, D. X. Zhu, H. T. Cao, Z. M. Su, J. Mater. Chem C 1 (2013) 1440.

[28] Z. Luo, X. Yuan, Y. Yu, Q. Zhang, D. T. Leong, J. Y. Lee, J. Xie, J. Am. Chem. Soc. 34 (2012) 16662.

[29] X. He, N. Zhu, V. W. W. Yam, Dalton Trans. 40 (2011) 9703.

[30] X. L. Xin, M. Chen, Y. B. Ai, F. L. Yang, X. L. Li, F. Y. Li, Inorg. Chem. 53 (2014) 2922.

[31] (a) M. T. Buckner, T. G. Matthews, F. E. Lytle, D. R. McMillin, J. Am. Chem. Soc. 101 (1979) 5846;
(b) J. R. Kirchhoff, D. R. Mcmillin, W. R. Robinson, D. R. Powell, A. T. Mckenzie, S. Chen, Inorg. Chem. 24 (1985) 3928.

[32] (a) D. G. Cuttell, S. M. Kuang, P. E. Fanwick, D. R. McMillin, R. A. Walton, J. Am. Chem. Soc. 124 (2002) 6;
(b) S. M. Kuang, D. G. Cuttell, D. R. McMillin, P. E. Fanwick, R. A. Walton, Inorg. Chem. 41 (2002) 3313.

[33] (a) C. L. Linfoot, M. J. Leitl, P. Richardson, A. F. Rausch, O. Chepelin, F. J. White, H. Yersin, N. Robertson, Inorg. Chem. 53 (2014) 10854;
(b) C. L. Linfoot, P. Richardson, T. E. Hewat, O. Moudam, M. M. Forde, A. Collins, F. White, N. Robertson, Dalton Trans. 39 (2010) 8945.

[34] (a) S. P. Luo, E. Mejía, A. Friedrich, A. Pazidis, H. Junge, A. Surkus, R. Jackstell, S. Denurra, S. Gladiali, S. Lochbrunner, M. Beller, Angew. Chem., Int. Ed. 52 (2013) 419;
(b) E. Mejía, S. P. Luo, M. Karnahl, A. Friedrich, S. Tschierlei, A. E. Surkus, H. Junge, S. Gladiali, S. Lochbrunner, M. Beller, Chem. Eur. J. 19 (2013) 15972;
(c) X. L. Chen, R. Yu, Q. K. Zhang, L. J. Zhou, X. Y. Wu, Q. Zhang, C. Z. Lu, Chem. Mater. 25 (2013) 3910;
(d) X. L. Li, X. L. Xin, Y. B. Ai, M. Tan, H. Lu, B. X. Du, Inorg. Chim. Acta 401 (2013) 58;
(e) H. Suh, D. J. Casadonte Jr., L. Hope-Weeks, H. J. Kim, B. Kim, T. Chang, Inorg. Chim. Acta 394 (2013) 710.

[35] (a) Q. Zhang, T. Komino, S. Huang, S. Matsunami, K. Goushi, C. Adachi, Adv. Funct. Mater. 22 (2012) 2327;
(b) X. Y. Xu, H. N. Xiao, Y. M. Xu, M. J. Zhang, Spectrochim. Acta, A 95 (2012) 427;
(c) X. L. Li, Y. B. Ai, B. Yang, J. Chen, M. Tan,; X. L. Xin, Y. H. Shi, Polyhedron 35 (2012) 47;
(d) I. Andrés-Tomé, J. Fyson, F. Baiao Dias, A. P. Monkman, G. Iacobellis, P. Coppo, Dalton Trans. 41 (2012) 8669;
(e) L. Zhang, S. Yue, B. Li, D. Fan, Inorg. Chim. Acta 384 (2012) 225;

(f) E. S. Smirnova, A. A. Melekhova, V. V. Gurzhiy, S. I. Selivanov, D. V. Krupenya, I. O. Koshevoy, S. P. Z. Tunik, Anorg. Allg. Chem. 638 (2012) 415.

[36] (a) C. W. Hsu, C. C. Lin, M. W. Chung, Y. Chi, G. H. Lee, P. T. Chou, C. H. Chang, P. Y. Chen, J. Am. Chem. Soc. 133 (2011) 12085;

(b) C. Wen, G. Tao, X. Xu, X. Feng, R. Luo, Spectrochim. Acta, A 79 (2011) 1345;

(c) R. D. Costa, D. Tordera, E. Qrti, H. J. Bolink, J. Schönle, S. Graber, C. E. Housecroft, E. C. Constable, J. A. Zampese, J. Mater. Chem. 21 (2011) 16108;

(d) R. Hou, T. H. Huang, X. J. Wang, X. F. Jiang, Q. L. Ni, L. C. Gui, Y. J. Fan, Y. L. Tan, Dalton Trans. 40 (2011) 7551.

[37] (a) J. C. Deaton, S. C. Switalski, D. Y. Kondakov, R. H. Young, T. D. Pawlik, D. J. Giesen, S. B. Harkins, A. J. M. Miller, S. F. Mickenberg, J. C. Peters, J. Am. Chem. Soc. 132 (2010) 9499;

(b) C. S. Smith, C. W. Branham, B. J. Marquardt, K. R. Mann, J. Am. Chem. Soc. 132 (2010) 14079;

(c) I. I. Vorontsov, T. Graber, A. Y. Kovalevsky, I. V. Novozhilova, M. Gembicky, Y. S. Chen, P. Coppens, J. Am. Chem. Soc. 131 (2009) 6566;

(d) L. Zhang, B. Li, Z. Su, Langmuir 25 (2009) 2068;

(e) L. Shi, B. Li, Eur. J. Inorg. Chem. 48 (2009) 2294;

(f) Q. Zhang, J. Ding, Y. Cheng, L. Wang, Z. Xie, X. Jing, F. Wang, Adv. Funct. Mater. 17 (2007) 2983;

(g) K. Saito, T. Arai, N. Takahashi, T. Tsukuda, T. Tsubomura, Dalton Trans. (2006) 4444.

[38] M. B. Duriska, S. M. Neville, J. Lu, S. S. Iremonger, J. F. Boas, C. J. Kepert, S. R. Batten, Angew. Chem., Int. Ed. 48 (2009) 8919.

[39] M. S. Wrighton, D. S. Ginley, D. L. Morse, J. Phys. Chem. 78 (1974) 2229.

[40] Rigaku. CrystalClear; Rigaku Corporation: Tokyo, Japan, 2009.

[41] Bruker. SAINT; Bruker AXS Inc.; Madison, Wisconsin, USA, 2009.

[42] Bruker. APEX2, SAINT and SADABS; Bruker AXS Inc., Madison, Wisconsin, USA, 2009.

[43] G. M. Sheldrick, SHELXL-97, Program for the Refinement of Crystal Structures; University of Göttingen: Göttingen, Germany, 1997.

[44] S. Samanta, S. Das, P. Biswas, J. Org. Chem. 78 (2013) 11184.

[45] H. M. Chen, F. Yue, H. Lin, H. K. Lin, Chin. J. Chinese U. 33 (2012) 1239.

[46] Y. Hattori, M. Nishikawa, T. Kusamoto, S. Kume, H. Nishihara, Inorg. Chem. 53 (2014) 2831.

[47] C. S. Smith, C. W. Branham, B. J. Marquardt, K. R. Mann, J. Am. Chem. Soc. 132 (2010) 14079.

Synthesis, Structures and Aggregation-Induced Emissive Properties of Copper(I) Complexes with 1H-imidazo[4,5-f][1,10]phenanthroline Derivative and Diphosphine as Ligands

Rong Liu, Miao-Miao Huang, Xi-Xi Yao, Hao-Huai Li, Feng-Lei Yang, Xiu-Ling Li*

Five mononuclear $[Cu(BIPP)(PP)]ClO_4$ (PP = dppe, **1**; dppp, **2**; bdpp, **3**; POP, **4**; xantphos, **5**) complexes with good phosphorescent emission were synthesized. Their photoluminescence quantum yields in the solid state increase with the increasing rigidity of diphosphine ligands and the increasing strength of intermolecular and intramolecular π···π interactions. The aggregation-induced emission of complexes **4** and **5** was investigated.

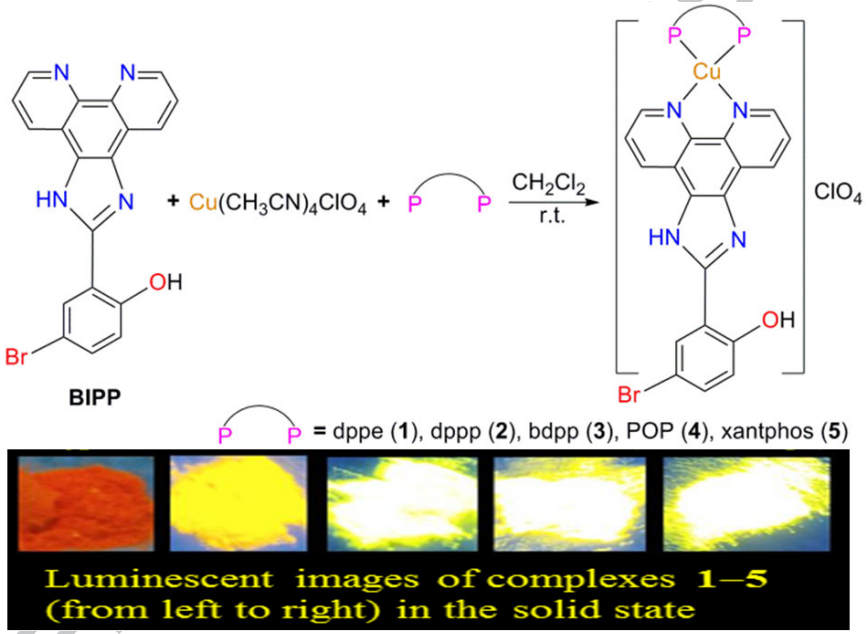

Synthesis, Structures and Aggregation-Induced Emissive Properties of Copper(I) Complexes with 1H-imidazo[4,5-f][1,10]phenanthroline Derivative and Diphosphine as Ligands

Highlights

1. Synthesized five Cu(I) complexes with good luminescence behaviour.
2. Analysized why such complexes are stable to air and moisture from crystallography.
3. Studied the luminescence lifetimes, quantum yields and aggregation-induced emission.